
How far actually is the Galactic Center IRS 13E3 from Sagittarius A* ?

Masato Tsuboi^{1,2}, Yoshimi Kitamura¹, Takahiro Tsutsumi³, Ryosuke Miyawaki⁴, Makoto Miyoshi⁵ and Atsushi Miyazaki⁶

¹Institute of Space and Astronautical Science, Japan Aerospace Exploration Agency,
3-1-1 Yoshinodai, Chuo-ku, Sagamihara, Kanagawa 252-5210, Japan

²Department of Astronomy, The University of Tokyo, Bunkyo, Tokyo 113-0033, Japan

³National Radio Astronomy Observatory, Socorro, NM 87801-0387, USA

⁴College of Arts and Sciences, J.F. Oberlin University, Machida, Tokyo 194-0294, Japan

⁵National Astronomical Observatory of Japan, Mitaka, Tokyo 181-8588, Japan

⁶Japan Space Forum, Kanda-surugadai, Chiyoda-ku, Tokyo, 101-0062, Japan

*E-mail: tsuboi@vsop.isas.jaxa.jp

Received (reception date); Accepted (acceptation date)

Abstract

The Galactic Center IRS 13E cluster is a very intriguing IR object located at ~ 0.13 pc from Sagittarius A* (Sgr A*) in projection distance. There are both arguments for and against the hypothesis that a dark mass like an intermediate mass black hole (IMBH) exists in the cluster. Recently we have detected the rotating ionized gas ring around IRS 13E3, which belongs to the cluster, in the H₃₀ α recombination line using ALMA. The enclosed mass is derived to be $M_{\text{encl.}} \simeq 2 \times 10^4 M_{\odot}$, which agrees with an IMBH and is barely less than the astrometric upper limit mass of the IMBH around Sgr A*. Because the limit mass depends on the true three-dimensional (3D) distance from Sgr A*, it is very important to determine it observationally. However, the 3D distance is indefinite because it is hard to determine the line-of-sight (LOS) distance by usual methods. We would attempt to estimate the LOS distance by spectroscopic informations. The CH₃OH molecule is easily destroyed by cosmic ray around Sgr A*. However, we detected a highly excited CH₃OH emission line in the ionized gas stream associated with IRS 13E3. This indicates that IRS 13E3 is located at $r \gtrsim 0.4$ pc from Sgr A*.

1 Introduction

The Galactic Center IRS 13E cluster, which was thought to contain several WR and O stars in the early observations (e.g. Genzel et al. 1996) is a very intriguing IR object located at ~ 0.13 pc from Sagittarius A* (Sgr A*) in projection distance. The common direction and similar amplitude of the proper motions of the member stars suggest that they are physically bound (e.g. Maillard et al. 2004) although the strong tidal force of Sgr A* should disrupt the cluster easily (e.g. Gerhard 2001). One of the possible speculations is that a dark mass like an intermediate mass black hole (IMBH), $M \sim 10^{4-5} M_{\odot}$, in the cluster would prevent the cluster disruption (e.g. Maillard et al. 2004). However, the upper limit mass of the IMBH around Sgr A* by long-term VLBA astrometry (Reid & Brunthaler 2004, Hansen & Milosavljević 2003) is derived to be $M \lesssim 3 \times 10^4 M_{\odot}$ if it is really located at the observed projection distance. Moreover, IR spectroscopic observations show that almost all the member stars in the cluster are not real stars but gas blobs. Therefore, such an IMBH is not always necessary (e.g. Schödel, Merritt, & Eckart 2009, Genzel et al. 2010).

However, the high concentration of the gas blobs itself is peculiar even in the Galactic center region. We consider that the existence of the IMBH in the IRS 13E cluster is still an open question. We searched ionized gas with a very large velocity width and compactness in order to prove this hypothesis. In our attempts, we had detected the ionized gas associated with IRS 13E3 in the H30 α recombination line using ALMA (Tsuboi et al. 2017b, Tsuboi et al. 2019). The enclosed mass of IRS 13E3 is derived to be $M_{\text{encl.}} \simeq 2.4 \times 10^4 M_{\odot}$, which agrees with the mass being an IMBH (Tsuboi et al. 2019). The derived mass is barely less than the astrometric upper limit mass if the 3D distance of IRS 13E3 is nearly equal to the projection distance.

The astrometric upper limit mass depends on the 3D distance from Sgr A*. However, the 3D distance is indefinite because the distance along the line-of-sight is hard to be derived by usual methods. The 3D distance may be much larger than the projection distance. We propose a new method to estimate the 3D distance from Sgr A*. Because the abundances of some molecules are considerably affected by the 3D distance, we would attempt to estimate the 3D distance by the spectroscopic informations of the molecules. First we searched the sign of the molecules in published data of the gas around the IRS 13E cluster. Throughout this paper, we adopt 8.2 kpc as the distance to the Galactic

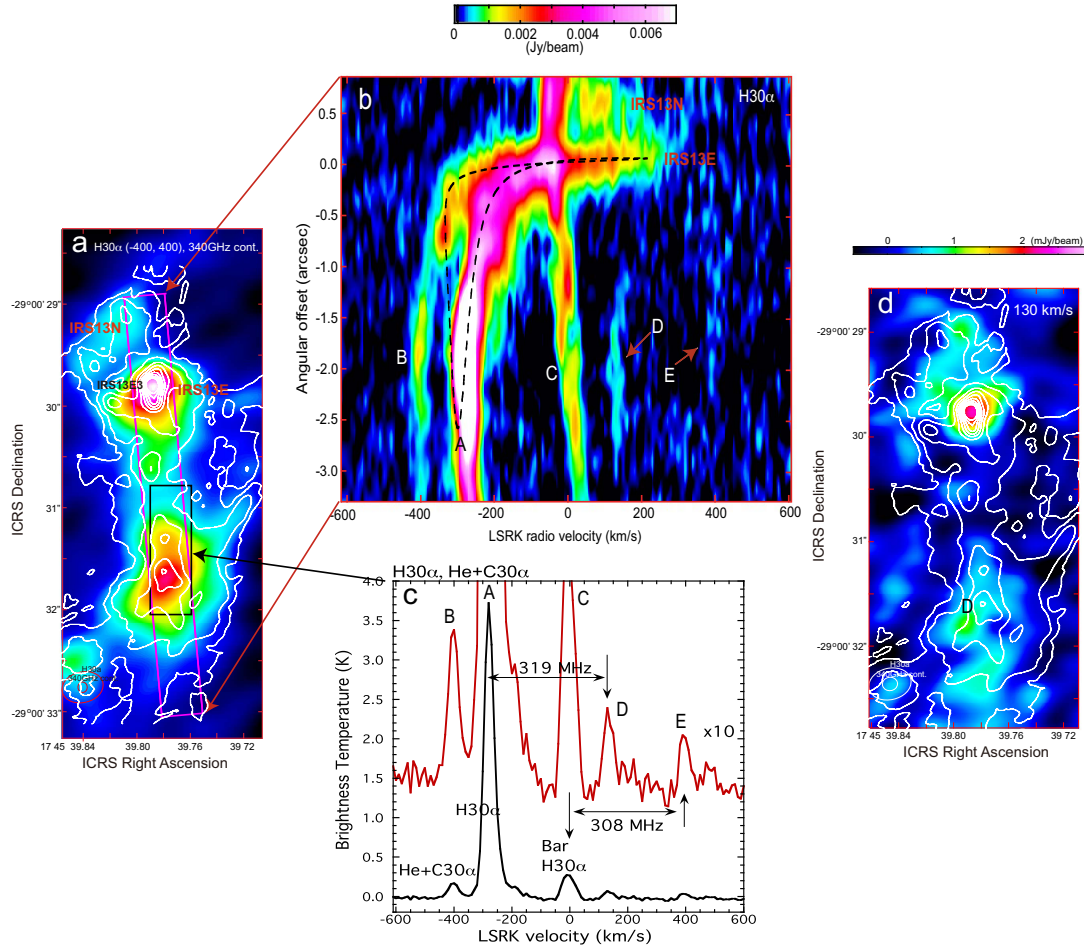


Fig. 1. **a** Continuum map at 340 GHz (contours) and moment 0 map in the H30 α recombination line (pseudocolor) of the IRS 13E cluster and the ionized gas stream depicted by a high-eccentricity Keplerian orbit (Tsuboi et al. 2017b). The integrated velocity range of the recombination line is $V_{\text{LSR}} = -400$ to 400 km s $^{-1}$. The angular resolutions are $0''.107 \times 0''.101$, $PA = -78^\circ$ for the continuum map and $0''.41 \times 0''.30$, $PA = -77^\circ$ in FWHM for the recombination line map, respectively. They are shown as the ovals at the lower left corner. **b** Position-velocity diagram in the H30 α recombination line along a red rectangular shown in **a**. The broken line shows the trajectory of the Keplerian orbit (Tsuboi et al. 2017b). **c** Line profile in the H30 α recombination line (black line) and ten-times magnification (red line). The sampling area is shown as a black rectangular shown in **a**. **d** Channel map in the H30 α recombination line with $V_{\text{LSR}} = 125$ to 135 km s $^{-1}$ (pseudocolor). The contours show the continuum map at 340 GHz.

center (e.g. Ghez et al. 2008, Gillessen et al. 2009, Schödel, Merritt, & Eckart 2009, Boehle et al. 2016): $1''$ corresponds to 0.04 pc or 8200 AU at the distance.

2 Search for the molecular emission line in the gas flows around the IRS 13E cluster

There are several published data with ALMA of the gas associated with the IRS 13 cluster (e.g. Moser et al. 2017, Tsuboi et al. 2018). First, we searched the sign of the easily found molecules like CO, CS, SiO and so on in the published data. However, we could not find the molecular gas (see also

Tsuboi et al. 2017a) although some authors have reported the detections of the molecular lines in the region within the circum-nuclear molecular disk (CND) (e.g. Moser et al. 2017, Yusef-Zadeh et al. 2017, Hsieh et al. 2019). The molecular gas would have a similar velocity feature in the PV diagram to that of the ionized gas if they are physically mixed in the same region. If so, the use of the velocity feature of the ionized gas as a template should be useful to find the sign of the molecular emission from the IRS 13 cluster.

Figure 1b is the position-velocity (PV) diagram along a red rectangular shown in Figure 1a. A feature labeled A is the ionized gas associated with IRS 13E3 in the H30 α recombination line ($\nu_{\text{rest}} = 231900.928$ MHz). While a feature labeled B is the counterpart in the He+C30 α recombination line (He30 α ; $\nu_{\text{rest}} = 231995.428$ MHz, C30 α ; $\nu_{\text{rest}} = 232016.636$ MHz). In addition, a feature labeled C is the ionized gas belonging to the "Bar" in the H30 α recombination line, which is an extended part of the "Galactic center mini-spiral"(GCMS). Finally, we detected a similar velocity feature, a feature labeled D, in the PV diagram to that of the ionized gas associated with IRS 13E3 in the H30 α recombination line. The line profiles of the area (a black rectangular shown in Figure 1a) are shown as Figure 1c. The line profiles of the features A, B, C and D are clearly identified as independent peaks. The frequency difference between the Gaussian-fit central frequencies of the features A and D is about $\Delta\nu \sim 318.7$ MHz. This corresponds to the velocity difference of $\Delta v \sim 412.3$ km s $^{-1}$. The rest frequency of the feature D is expected to be $\nu_{\text{rest}} = 231582.2$ MHz. The candidate transitions corresponding to the rest frequency are summarized in Table 1. The frequency difference and velocity difference from the feature A of the feature D are also summarized in Table 1.

There are three transitions of CH₃OH $v = 1$, 17(6,11)-17(7,10), CH₃¹³CH₂CN 26(3,24)-25(3,23), and CH₃CHO 12(3,10)-11(3,9)A₊₊ within $\Delta V = \pm 25$ km s $^{-1}$ from the velocity of the feature D, $V_{\text{LSR}} \sim 134$ km s $^{-1}$ (see Figure 1c). These are the candidate transitions of the feature D because features A and D have wide FWHM velocity widths of $\Delta V_{\text{FWHM}} = 50$ and 46 km s $^{-1}$, respectively: the half width of the feature A is used as the tolerance mentioned above. ¹³CH₃CH₂CN, CH₃¹³CH₂CN, and CH₃CH₂¹³CN molecules are isotope-substituted molecules of CH₃CH₂CN. These molecules are in a family formed so that Carbon atoms, C, located at different positions are substituted by Carbon isotope atoms, ¹³C. The intensities of these emission lines are observed to be similar in warm and dense molecular clouds, for example, in Orion Molecular Cloud (e.g. Demyk et al. 2007). Therefore, if the feature D is the CH₃¹³CH₂CN 26(3,24)-25(3,23) emission line, the other emission lines should be also observed in some degree around $V_{\text{LSR}} \sim 30$ and ~ 50 km s $^{-1}$. However, there is no sign in Figure 1c. The transition presumably is not the feature D.

Next we discuss the third candidate transition. CH₃CHO molecule has another transition, CH₃CHO 12(-3,10)-11(-3,9)E ($\nu_{\text{rest}} = 231748.722$ MHz) in the frequency range, which corresponds

Table 1. Candidate transitions corresponding to the feature D.

Name	transition	Rest frequency	Frequency difference	Velocity difference	Remarks
		ν_{rest} [MHz]	$\Delta\nu$ [MHz]	ΔV [km s ⁻¹]	
Hydrogen atom	H30 α	231900.928	–	–	
t-CH ₃ CH ₂ OH	21(5,17)-21(4,18)	231558.513*	–342.415	443.0	$T_{\text{R}} = 1.5$ K at Sgr B2 (N) [‡]
t-CH ₃ CH ₂ OH	21(5,16)-20(4,17)	231560.877*	–340.051	439.9	–
CH ₃ OH $v = 1$	17(6,11)-17(7,10)	231589.972 [‡]	–310.956	402.3	has not been observed
CH ₃ ¹³ CH ₂ CN	26(3,24)-25(3,23)	231590.269*	–310.659	401.9	$T_{\text{R}} = 0.6$ K at OriMC-1 [†]
CH ₃ CHO	12(3,10)-11(3,9)A ₊₊	231595.269*	–305.659	395.4	$T_{\text{R}} = 6.0$ K at Sgr B2 (N) [‡]
CH ₃ CH ₂ ¹³ CN	26(3,24)-25(3,23)	231646.312*	–254.616	329.4	$T_{\text{R}} = 0.3$ K at OriMC-1 [†]
CH ₃ OCHO	27(3,25)-27(2,26)A	231657.892*	–243.036	314.4	$T_{\text{R}} = 2.4$ K at Sgr B2 (N) [‡]
¹³ CH ₃ CH ₂ CN	26(3,24)-25(3,23)	231662.964*	–237.964	307.8	$T_{\text{R}} = 0.4$ K at OriMC-1 [†]
CH ₃ CHO	12(-3,10)-11(-3,9)E	231748.722*	–152.206	196.9	$T_{\text{R}} = 6.2$ K at Sgr B2 (N) [‡]
Feature D	–	231582.2	–318.7	412.3	
Feature E	–	231592.5	–308.9 [‡]	398.9 [‡]	

* <https://physics.nist.gov/cgi-bin/micro/table5/start.pl>. [†] Demyk et al. 2007. [‡] Nummelin et al. 1998. [‡] Li-Hong & Lovas 1997. ^{||} from the feature A. [‡] from the feature C.

to the velocity difference of $\Delta V = 196.9$ km s⁻¹ from the feature A. Because these transition parameters are similar, the intensities of these emission lines are observed to be similar in warm and dense molecular clouds, for example, in Sgr B2(N) (e.g. Nummelin et al. 1998). Therefore, if the feature D is the transition of the CH₃CHO molecule, the CH₃CHO 12(-3,10)-11(-3,9)E emission line should be also observed in some degree around $V_{\text{LSR}} \sim -80$ km s⁻¹. However, there is no sign in Figure 1c. The transition presumably is not the feature D.

Finally, it is most probable that we detect the vibrationally excited CH₃OH emission line as the counterpart of the feature D. If this is the case, we have the first detection of the CH₃OH $v = 1$, 17(6,11)-17(7,10) emission line ($\nu_{\text{rest}} = 231589.972$ MHz, Li-Hong & Lovas 1997). Figure 1d shows the feature D in the channel map of $V_{\text{LSR}} = 130$ km s⁻¹ referencing to the H30 α recombination line, which corresponds to $V_{\text{LSR}} \sim -270$ km s⁻¹ referencing to the CH₃OH $v = 1$ emission line. The velocity width is $\Delta V = 10$ km s⁻¹. The feature can be identified up to $\delta_{\text{ICRS}} = -29^{\circ}00'31''$ along the ionized gas stream depicted by a high-eccentricity Keplerian orbit (Tsuboi et al. 2017b).

The CH₃OH molecule is reported to be destroyed easily through the cosmic-ray photodissoci-

ation reaction; $\text{CH}_3\text{OH} + c.r. \rightarrow \text{H}_2\text{CO} + \text{H}_2$ (e.g. Harada et al. 2015). Because the cosmic ray intensity is thought to increase significantly with approaching to Sgr A*, CH_3OH molecule does not survive within some limit radius. This is probably why the CH_3OH emission of the CN2 is very weak (see fig. 1e in Tsuboi et al. 2018). The limit radius is expected to be at least $r \sim 1$ pc from the projection distance of the innermost component of the CN2 in the CH_3OH emission line (Tsuboi et al. 2018). Therefore the detection of the CH_3OH emission line in the gas streamer suggests that the streamer is located at the 3D distance of $r \gtrsim 1$ pc from Sgr A*. Because the gas streamer is associated physically with IRS 13E3, IRS 13E3 is also located at a similar 3D distance from Sgr A*, which is farther than the projection distance, $r_p \sim 0.13$ pc. If so, the astrometric upper limit mass becomes larger and increases the possibility that an IMBH exists in the IRS 13E cluster.

In addition, there is also a faint feature labeled E at $V_{\text{LSR}} = 399$ km s⁻¹ in figure 1c. Because the frequency difference between the Gaussian-fit central frequencies of the features C and E is about $\Delta\nu \sim 308.9$ MHz or the velocity difference is $\Delta V \sim 398.9$ km s⁻¹, this is presumably the CH_3OH $v = 1$, 17(6,11)-17(7,10) emission line corresponding to the feature C at $V_{\text{LSR}} \sim -5$ km s⁻¹. As mentioned above, the feature C corresponds to the "Bar" of the GCMS. The "Bar" is thought to obey a nearly pole-on high-eccentricity Keplerian orbit around Sgr A* (Tsuboi et al. 2017a), and the part with $V_{\text{LSR}} \sim 0$ km s⁻¹ corresponds to the vicinity of the apoastron of the orbit. The 3D distance from Sgr A* at the apoastron was estimated to be $a(1+e) \sim 0.9$ pc. The 3D distance is consistent with the detection of the CH_3OH $v = 1$, 17(6,11)-17(7,10) emission line there.

3 Vibrationally excited CH_3OH emission in the Northern arm

We searched another example of the appearance and disappearance of the CH_3OH $v = 1$ emission line in the GCMS. Figure 2a shows the moment 0 map in the $\text{H}30\alpha$ recombination line with the integrated velocity range of $V_{\text{LSR}} = -400$ to 400 km s⁻¹ (contours) and the channel map of $V_{\text{LSR}} = -55$ to -45 km s⁻¹ (pseudocolor). Figure 2b is the PV diagram in the $\text{H}30\alpha$ recombination line along the Northern arm (NA) of the GCMS (a red rectangular shown in Figure 2a). The Northern arm is appeared as a long curved ridge in the diagram (a black broken line in Figure 2b). There may be a faint feature corresponding to He+C30 α recombination line of the NA. As mentioned previously, the molecular gas would have a similar velocity feature in the PV diagram to that of the ionized gas if they are physically related to each other in the same region. Note that a long but faint curved ridge is identified in the diagram (a white broken line in Figure 2b). Because the velocity feature of the ridge is similar to the feature in the $\text{H}30\alpha$ recombination line and the velocity difference of $\Delta V \sim 400$ km s⁻¹ between the two ridges is the same as that discussed in the previous section, this probably

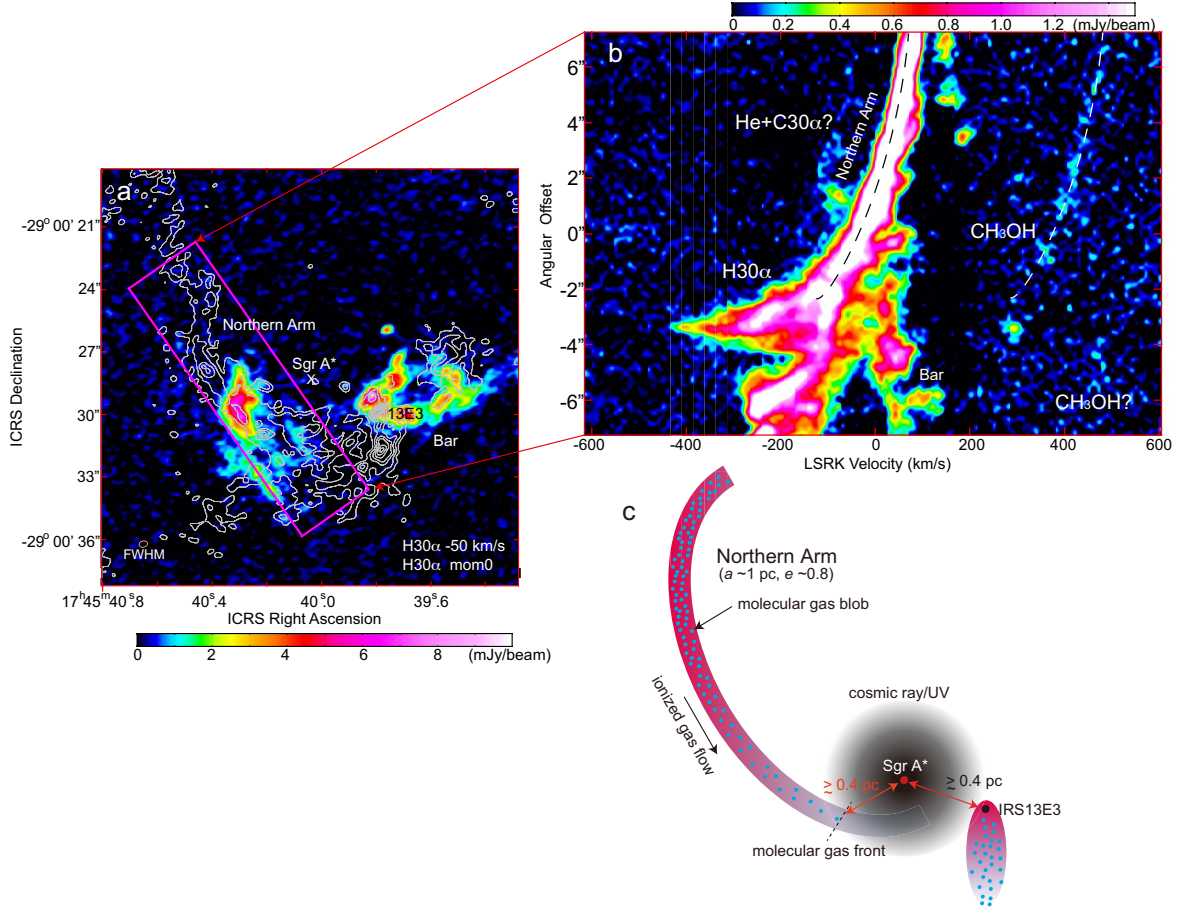


Fig. 2. **a** Moment 0 map in the H30 α recombination line with the integrated velocity range of $V_{\text{LSR}} = -400$ to 400 km s^{-1} (contours) and channel map of $V_{\text{LSR}} = -55$ to -45 km s^{-1} (pseudocolor). The angular resolution is $0''.41 \times 0''.30$, $PA = -77^\circ$, which is shown as the oval at the lower left corner. The white cross shows the position of Sgr A*. **b** Position-velocity diagram in the H30 α recombination line along the Northern arm (a red rectangular shown in a). **c** Schematic display of the positional relation among Sgr A*, IRS 13E3, and the Northern Arm.

corresponds to the CH₃OH $v = 1$ emission line.

The ridge in the CH₃OH $v = 1$ emission line is disappeared around the angular offset of $\Delta\theta \sim -1''$. The apparent velocity at the disappearance point is $V_{\text{LSR}} \sim 350 \text{ km s}^{-1}$. This corresponds to the ionized gas component with $V_{\text{LSR}} \sim -50 \text{ km s}^{-1}$ (see Figure 2a). Although the projection distance from Sgr A* of the disappearance point is $\theta_p \sim -3''$ or $r_p \sim 0.1 \text{ pc}$, the 3D distance may be larger than the projection distance because this component is located at just before the intense acceleration from $V_{\text{LSR}} \sim -50$ to $\lesssim -200 \text{ km s}^{-1}$. Assuming the trajectory of the NA is described by a Keplerian orbit with the semi-major axis of $a \sim 1 \text{ pc}$, the eccentricity of $e \sim 0.8$, and the inclination angle of $i \sim 140^\circ$ (Zhao et al. 2009), the 3D distance of the disappearance point (molecular gas front) is estimated to be $r \sim 0.4 \text{ pc}$ (please see figure 2c). The NA is rapidly approaching to Sgr A* although the CND is rotating in a circular orbit around it. The elapse time moving from $r \sim 1 \text{ pc}$ to $r \sim 0.4 \text{ pc}$ is $\sim (1 - 2) \times 10^3 \text{ yr}$. The gradual decay would be why CH₃OH molecule is survived up to $r \sim 0.4$

pc. It is assumed here that IRS 13E3 is located at $r \gtrsim 0.4$ pc. Nevertheless the astrometric upper limit mass increases up to $\sim 4 \times 10^4 M_{\odot}$ (Reid&Brunthaler 2004, Hansen & Milosavljević 2003), which is fairly larger than the estimated mass of IRS 13E3 (Tsuboi et al. 2019).

Acknowledgments

This work is supported in part by the Grant-in-Aid from the Ministry of Education, Sports, Science and Technology (MEXT) of Japan, No.19K03939. The National Radio Astronomy Observatory (NRAO) is a facility of the National Science Foundation operated under cooperative agreement by Associated Universities, Inc. USA. ALMA is a partnership of ESO (representing its member states), NSF (USA) and NINS (Japan), together with NRC (Canada), NSC and ASIAA (Taiwan), and KASI (Republic of Korea), in cooperation with the Republic of Chile. The Joint ALMA Observatory (JAO) is operated by ESO, AUI/NRAO and NAOJ. This paper makes use of the following ALMA data: ADS/JAO.ALMA#2015.1. 01080.S and ALMA#2017.1.00503.S.

References

- Boehle, A. et al. 2016, ApJ, 830, 17
- Demyk, K., Mäder, H., Tercero, B., Cernicharo, J., Demaison, J., Margulès, L., Wegner, M., Keipert, S., Sheng, M. 2007, A&A, 466, 255
- Genzel, R., Thatte, N., Krabbe, A., Kroker, H., & Tacconi-Garman, L. E. 1996, ApJ, 472, 153
- Genzel, R., Eisenhauer, F., & Stefan Gillessen, S. 2010, *Rev. Mod. Phys.*, 82, 3121
- Gerhard, O., 2001, ApJL, 546, L39
- Ghez, A. M., et al. 2008, ApJ, 689, 1044
- Gillessen, S., Eisenhauer, F., Trippe, S., Alexander, T., Genzel, R., Martins, F., & Ott, T. 2009, ApJ, 692, 1075
- Gravity Collaboration, 2018, A&A, 615, L15
- Hansen, B. M. S. & Milosavljević, M., 2003, ApJL, 593, L77
- Harada, N., Riquelme, D., Viti, S. et al. 2015, A&A, 584, A102
- Hsieh, P.-Yi., Koch, P. M., Kim, W.-T., Ho, P.T. P., Yen, H.-W., Harada, N., & Tang, Y.-W., 2019, ApJL, 885, L20
- Li-Hong, Xu & Lovas, F.J. 1997, Journal of Physical and Chemical Reference Data, 26, 17, <https://doi.org/10.1063/1.556005>
- Maillard, J. P., Paumard, T., Stolovy, S. R., & Rigaut, F. 2004, A&A, 423, 155
- Moser, L., Sánchez-Monge, Á., Eckart, A., Requena-Torres, M. A., García-Marin, M., Kunneriath, D., Zensus, A., Britzen, S., Sabha, N., Shahzamanian, B., Borkar, A., & Fischer, S.
- Nummelin, A., Bergman, P., Hjalmarson, Å., Friberg, P., Irvine, W. M., Millar, T. J., Ohishi, M., & Saito, S., 1998, ApJS, 117, 427
- Reid, M. J. & Brunthaler, A. 2004, ApJ, 616, 872

Schödel, R., Merritt, D. & Eckart, A., 2009, *A&A*, 502, 91

Tsuboi, M., Kitamura, Y., Uehara, K., Miyawaki, R., Tsutsumi, T., Miyazaki, A., & Miyoshi, M., 2017, *ApJ*, 842, id. 94

Tsuboi, M., Kitamura, Y., Tsutsumi, T., Uehara, K., Miyoshi, M., Miyawaki, R., & Miyazaki, A., 2017b, *ApJL*, 850, id L5

Tsuboi, M., Kitamura, Y., Uehara, K., Tsutsumi, T., Miyawaki, R., Miyoshi, M., & Miyazaki, A., 2018, *PASJ*, 70, id 85

Tsuboi, M., Kitamura, Y., Tsutsumi, T., Miyawaki, R., Miyoshi, M., & Miyazaki, A., 2019, *PASJ*, 71, id 105

Yusef-Zadeh, F., Wardle, M., Kunneriath, D., Royster, M., Wootten, A., & Roberts, D. A., 2017, *ApJL*, 850, id L30.

Zhao, J.-H., Morris, M. R., Goss, W. M., An, T., 2009, *ApJ*, 699,186